Interactive effects of light, nitrogen source, and carbon dioxide on energy metabolism in the diatom Thalassiosira pseudonana

ARTICLE · JULY 2015

DOI: 10.1002/lno.10134

7 AUTHORS, INCLUDING:

Dalin Shi
Xiamen University
15 PUBLICATIONS **431** CITATIONS
SEE PROFILE

Weiying Li
Xiamen University
1 PUBLICATION **1** CITATION
SEE PROFILE

Shuh-JI Kao
Xiamen University
18 PUBLICATIONS **188** CITATIONS
SEE PROFILE

LIMNOLOGY
and
OCEANOGRAPHY

ASLO

Limnol. Oceanogr. 00, 2015, 00–00

doi: 10.1002/lno.10134

Interactive effects of light, nitrogen source, and carbon dioxide on energy metabolism in the diatom *Thalassiosira pseudonana*

Dalin Shi,[†*1,2] Weiying Li,[†1] Brian M. Hopkinson,[3] Haizheng Hong,[1,2] Dongmei Li,[1] Shuh-Ji Kao,[1] Wenfang Lin[1]

[1]State Key Laboratory of Marine Environmental Science, Xiamen University, Xiamen, Fujian, P. R. China
[2]Key Laboratory of the Ministry of Education for Coastal and Wetland Ecosystems, Xiamen University, Xiamen, Fujian, P. R. China
[3]Department of Marine Sciences, University of Georgia, Athens, Georgia

Abstract

Due to the ongoing effects of climate change, phytoplankton are likely to experience enhanced irradiance, more reduced nitrogen, and increased water acidity in the future ocean. Here, we used *Thalassiosira pseudonana* as a model organism to examine how phytoplankton adjust energy production and expenditure to cope with these multiple, interrelated environmental factors. Following acclimation to a matrix of irradiance, nitrogen source, and CO_2 levels, the diatom's energy production and expenditures were quantified and incorporated into an energetic budget to predict how photosynthesis was affected by growth conditions. Increased light intensity and a shift from NO_3^- to NH_4^+ led to increased energy generation, through higher rates of light capture at high light and greater investment in photosynthetic proteins when grown on NH_4^+. Secondary energetic expenditures were adjusted modestly at different culture conditions, except that NO_3^- utilization was systematically reduced by increasing pCO_2. The subsequent changes in element stoichiometry, biochemical composition, and release of dissolved organic compounds may have important implications for marine biogeochemical cycles. The predicted effects of changing environmental conditions on photosynthesis, made using an energetic budget, were in good agreement with observations at low light, when energy is clearly limiting, but the energetic budget over-predicts the response to NH_4^+ at high light, which might be due to relief of energetic limitations and/or increased percentage of inactive photosystem II at high light. Taken together, our study demonstrates that energetic budgets offered significant insight into the response of phytoplankton energy metabolism to the changing environment and did a reasonable job predicting them.

Introduction

Human activities such as fossil fuel combustion and deforestation have caused atmospheric carbon dioxide (CO_2) levels to rise by roughly 40% over the past 250 yr and atmospheric CO_2 is predicted to reach 800 ppm by the end of this century if anthropogenic emissions continue unabated (Orr et al. 2005). Rising atmospheric CO_2 will bring about a host of changes to the physics and chemistry of the ocean that will likely lead to various direct or indirect effects on marine phytoplankton. The ocean will warm from the surface causing changes in water circulation and mixing. An increase in temperature should accelerate the rate of many biological processes in marine phytoplankton. However, it is thought that sea surface warming may have the most profound effects on phytoplankton through augmenting the stratification of surface waters, resulting in a decrease in the upward flux of nutrients such as nitrate (NO_3^-) from deep waters (Doney 2006). Meanwhile, an increase in sea surface temperature will cause shoaling of the mixed layer leading to an increase in the average light intensity for phytoplankton cells (Behrenfeld et al. 2006; Doney 2006).

The chemical changes resulting from the dissolution of anthropogenic CO_2 in the surface ocean, collectively referred to as ocean acidification (Caldeira and Wickett 2003; Doney et al. 2009), may affect marine phytoplankton via different processes. For example, higher CO_2 concentrations in seawater stimulate rates of photosynthesis and growth in many phytoplankton (e.g., Tortell et al. 2008; Gao and Campbell 2014). Concomitantly, decreasing pH may indirectly affect phytoplankton by altering the acid-base chemistry and, therefore, the availability of trace metals such as iron and

Additional Supporting Information may be found in the online version of this article.

[†]These authors contribute equally to this work.
*Correspondence: dshi@xmu.edu.cn

zinc (Breitbarth et al. 2010; Shi et al. 2010; Xu et al. 2012). Aside from micronutrients, ocean acidification could also change the nitrogenous nutrition of phytoplankton by inhibiting ammonia oxidation in the upper layers of the ocean (Huesemann et al. 2002; Beman et al. 2011), which, together with less input of NO_3^- from deep waters and more atmospheric anthropogenic ammonium (NH_4^+) deposition (Doney 2006; Duce et al. 2008), would shift the chemical form of nitrogen (i.e., NO_3^- vs. NH_4^+) supplied to phytoplankton in the surface ocean.

As our planet progresses further into the anthropocene, marine phytoplankton are likely to be confronted with a rise in CO_2 concentrations, as CO_2 released in the atmosphere dissolves into the ocean, increased light intensities, as warming further stratifies surface waters, and changes in nutrient availability, including nitrogen, again due to increased stratification and changes in N cycling. It has increasingly been recognized that the effects of these variables must be examined in concert to help understand how the marine biota will respond to global change. However, predicting the net effect of these multiple, interconnected changes on biogeochemically relevant variables such as growth and photosynthetic rates is challenging, and a wide range of approaches have been put forward. Major challenges that must be addressed include the diversity of organismal responses to single and multiple environmental perturbations, ecological interactions, and evolutionary dynamics that may alter an organism's responses to environmental change (Boyd and Hutchins 2012; Collins et al. 2014). Approaches to dealing with this diversity of responses to multiple environmental parameters include focusing on the typical responses of organisms within a functional group (Boyd et al. 2010), thorough study of key or model species (Schaum et al. 2013), and model approaches that consider a span of possible behaviors among different species to determine which will thrive in a future ocean (Litchman et al. 2012; Dutkiewicz et al. 2013). These approaches have various advantages and disadvantages. For example, using a long-standing and useful categorization scheme, the functional group approach allows the effects of global change to be integrated into existing frameworks and models, but inevitably ignores variations in responses that may occur within groups. Exhaustive study of individual species captures some of that variation, but is labor intensive and can only be applied to a small number of phytoplankton species.

An additional approach is to take a holistic view of organismal metabolism examining the ways in which environmental change alters the use of limiting materials or energy (Halsey and Jones 2015). Energetic and materials budgets are widely used in ecology to predict how environmental variables alter an organism's performance (e.g., Sousa et al. 2008; Nisbet et al. 2012). They offer a common framework for handling the diverse traits, life-history characteristics, and metabolic capabilities of different organisms. However, these approaches have been used infrequently in assessing the effects of global change on the pelagic ecosystem, and have generally only been applied to single factor experiments (Hopkinson et al. 2011; Eichner et al. 2014). One exception to this was a study by Muller and Nisbet (2014) where they used a dynamic energy budget model to show that multiple components of the oceanic CO_2 system affect growth and calcification in *Emiliania huxleyi*, demonstrating the utility of this approach.

In this study, we chose the model diatom species *Thalassiosira pseudonana* to investigate the interrelated effects of light, nitrogen source, and CO_2 on light energy harvesting and cellular metabolism as the effects of these factors have been studied individually in this organism but the full extent of interactions among these factors have yet to be examined. Key processes involved in carbon metabolism, nitrogen assimilation, and photorespiration in the diatom were assessed systematically using physiological, biochemical and molecular approaches to seek a mechanistic understanding of how marine phytoplankton would balance energy harvesting and dissipation to cope with the changing environment likely encountered in the future ocean. An energetic budget for the organism was constructed and used to make predictions about the effects of changes in growth conditions on photosynthesis, and these predictions were compared with the experimental results.

Methods

Cell culturing and experimental design

The marine diatom *T. pseudonana* (CCMP 1335) was obtained from the Provasoli-Guillard National Center for Marine Algae and Microbiota. Cells were grown in 0.22 μm-filtered and microwave-sterilized oligotrophic South China Sea surface water enriched with Aquil* concentrations of phosphate, silicate, trace metals, and vitamins (Sunda et al. 2005) and with 100 μmol L^{-1} of either NO_3^- or NH_4^+ as the nitrogen source. All chemicals used were purchased from Sigma-Aldrich Chemical. Cultures were maintained at 20°C under continuous light in an AL-41L4 algae chamber (Percival). Although continuous light is not environmentally realistic, it helps simplify our full factorial experiment with three factors (i.e., light intensity, nitrogen source, and CO_2 level, Table 1) and is commonly used by similar mechanistic studies (e.g., Parker and Armbrust 2005). Cell number was determined daily using a Z2 Coulter Counter (Beckman Coulter), and specific growth rates were calculated from the linear regressions of natural logarithm of cell number vs. time for the exponential phase of growth. Sterile technique was applied for culturing and experimental manipulations.

T. pseudonana was first grown under each of four conditions representing a matrix of nitrogen source (NO_3^- or NH_4^+) and light intensity (30 or 250 μmol photos m^{-2} s^{-1}, LL or HL, respectively) for over 2 months (Table 1).

Table 1. Treatment names, experimental growth conditions, and carbonate chemistry for each light, CO_2 and N treatment. Alkalinity and pCO_2 were calculated from pH_T, DIC, temperature, salinity, [PO_4^{3-}] and [SiO_4^{2-}] using the CO2Sys program (Pierrot et al. 2006) with equilibrium constants K_1 and K_2 in Mehrbach et al. (1973) refit by Dickson and Millero (1987). Errors denote 1 SD ($n = 3$).

Treatment name	Light μmol photons m^{-2} s^{-1})	pCO_2 (μatm)	Nitrogen source	pH_T	DIC (μmol kg^{-1})	Alkalinity (μmol kg^{-1})	pCO_2 (μatm)
LL400NO_3^-	30	400	Nitrate	8.03 ±0.01	2400 ± 6	2695 ± 2	484 ± 10
LL800NO_3^-	30	800	Nitrate	7.83 ± 0.00	2527 ± 4	2713 ± 6	838 ± 1
LL400NH_4^+	30	400	Ammonium	8.03 ± 0.02	2384 ± 14	2674 ± 2	489 ± 21
LL800NH_4^+	30	800	Ammonium	7.82 ± 0.00	2530 ± 4	2710 ± 4	867 ± 1
HL400NO_3^-	250	400	Nitrate	8.06 ± 0.00	2362 ± 8	2669 ± 9	449 ± 2
HL800NO_3^-	250	800	Nitrate	7.84 ± 0.01	2482 ± 56	2674 ± 48	797 ± 4
HL400NH_4^+	250	400	Ammonium	8.06 ± 0.01	2353 ± 3	2660 ± 1	448 ± 9
HL800NH_4^+	250	800	Ammonium	7.84 ± 0.00	2463 ± 8	2657 ± 8	779 ± 3

Following acclimation to nitrogen source and light intensity, the cultures were maintained semi-continuously under each of the two CO_2 levels (i.e., 400 and 800 μatm, Table 1) obtained by gentle bubbling with humidified and 0.22 μm-filtered CO_2-air mixtures generated by CO_2 mixers (Ruihua Instrument & Equipment Ltd). When the slopes of three or more consecutive growth curves, which corresponded to a total cell generation ≥ 25, were not significantly different (F-test), the culture was considered acclimated to the experimental treatments. Triplicate cultures of the acclimated cells were then grown in 1 L polycarbonate bottles (Nalgene Labware) for another six generations and harvested for analysis in mid-exponential phase when the diatom cells were at steady-state, as verified by tracking the photochemical quantum yield of photosystem II (PSII; F_v/F_m) over time, and nutrient concentrations were well-above the half-saturation constants (1–10 μ mol L^{-1} for NO_3^-, Mulholland and Lomas 2008; $\sim$ 40 nmol L^{-1} for NH_4^+, Sunda and Hardison 2007) for growth and uptake, which however can vary with physiological state, nutrient prehistory, and phytoplankton species (Mulholland and Lomas 2008).

Carbonate chemistry in media

Carbonate chemistry in culture media was manipulated by bubbling with humidified CO_2-enriched air (400 or 800 μatm CO_2). The pH_T (pH on the total scale) of media was monitored daily throughout the experimental period using a spectrophotometric method (Zhang and Byrne 1996), and drifted by < 0.1 units by the end of the experiment. The dissolved inorganic carbon (DIC) concentration was analyzed by acidification and subsequent quantification of released CO_2 with a CO_2 analyzer (LI 7000, Apollo SciTech). Calculations of alkalinity and pCO_2 were made using the CO2Sys program (Pierrot et al. 2006) based on measurements of pH_T and DIC using the carbonic acid dissociation constants of Mehrbach et al. (1973) that were refit in different functional forms by Dickson and Millero (1987). Carbonate chemistry of the different experimental treatments is shown in Table 1.

Elemental composition

To determine cellular carbon and nitrogen quota, 6×10^6 cells were collected onto 25 mm precombusted GF/F filters and stored at −80°C. For analysis, the filters were dried overnight at 60°C, exposed to fuming HCl for 6 h to remove inorganic carbon, dried overnight again at 60°C, and then packed in tin cups before analysis on a PerkinElmer Series II CHNS/O Analyzer 2400.

Nitrate reductase activity

Nitrate reductase (NR) activity was assayed using the spectrophotometric method for the detection of NO_3^- reduction to the formation of NO_2^- (Berges and Harrison 1995a; Lomas 2004). Briefly, 1×10^7 cells was collected by gentle filtration and the filter was ground completely on ice in 1 mL of homogenization buffer (200 mmol L^{-1} phosphate buffer, pH 7.9; 1 mmol L^{-1} dithiothreitol; 0.3% w/v polyvinyl pyrrolidone; 0.1% v/v Triton X-100; 3% v/v bovine serum albumin; 5 mmol L^{-1} EDTA), clarified at 1000 × g for 5 min by centrifugation at 4°C. The resulting supernatant (each aliquot of 0.4 mL) was added to 0.45 mL of freshly prepared reaction buffer (20 mmol L^{-1} phosphate buffer, pH 7.9; 0.2 mmol L^{-1} NADH; 10 mmol L^{-1} KNO_3). Enzyme activity in two tubes was immediately terminated by the addition of 0.375 mL cold ethanol and 0.375 mL of 300 mmol L^{-1} zinc acetate and served as blanks, while the other two tubes were incubated at 20°C for 30 min before the reaction was terminated. Samples were centrifuged at 12,000 × g for 5 min and then 3 μL of 0.83 mmol L^{-1} phenazine methosulfate was added to the supernatant to oxidize any residual NADH. The NO_2^- concentration in the supernatant was measured colormetrically after reacting with sulfanilamide and *N*-(1-naphtyl)-ethylenediamine dihydrochloride for 30 min, and absorbance of the resulting reaction mixtures was measured at the wavelength of 543 nm. The activity of NR was calculated from NO_2^- production during the incubation (after correcting for NO_2^- contamination by subtraction with the

blanks) and normalized to the total number of cells collected on the filter.

Fatty acid analysis

Fatty acid composition in cells was determined by a one-step extraction and transesterification process (Rodriguez-Ruiz et al. 1998; Frada et al. 2013). Briefly, 6×10^6 cells were collected onto precombusted GF/F filters and lyophilized completely to remove the excess moisture. The samples were heated at 80°C for 1 h in the presence of 2 mL of acetyl chloride: methanol mixture (1:20, v/v) and 1 mL of hexane. Heptadecanoic acid (10 μg) was added to each sample prior to heating as an internal standard and to check for transesterification efficiency. Subsequently, 1 mL of Milli-Q water was added to each sample after cooling down to room temperature. After shaking and phase separation, the top hexane phases were recovered and the lower phase was extracted again with 1 mL of hexane. The hexane phases were combined and dried under N_2 stream and then redissolved in 0.5 mL of hexane for sample analysis on a gas chromatography-mass spectrometer (Agilent 6890N/5975B, Agilent Technologies). The elution was performed on an Agilent DB-5ms capillary column (30 m $\times$ 0.22 μm) which was heated from 140 to 250°C at 4°C min^{-1}. Fatty acid methyl esters were identified by reference to authentic standards (Supelco^{TM} 37 component FAME, Sigma Aldrich) processed under the same analytical conditions.

***β*-1,3-glucan analysis**

Cellular β-1,3-glucan was extracted by diluted H_2SO_4 and determined colormetrically by phenol-sulphuric acid method (Granum and Myklestad 2002). Briefly, 6×10^6 cells were collected onto precombusted GF/F filters and the filters were extracted by 4 mL of 0.05 mol L^{-1} H_2SO_4 at 60 °C for 10 min. The extract was then centrifuged at 12,000 $\times$ *g* for 5 min and an aliquot (0.4 mL) of the supernatant was mixed with 0.1 mL of 3% aqueous phenol solution and 1 mL of concentrated H_2SO_4. The reaction mixture was immediately mixed by vortex. The sample tube was allowed to stand for 30 min and cooled in water bath (20°C), and the absorption was then measured at the wavelength of 485 nm. The amount of reducing sugar was calculated using glucose as the standard. A correction for the weight of nonhydrolyzed β-1,3-glucan was made by a factor of 0.9 (Granum and Myklestad 2002).

Western blotting

T. pseudonana cells were collected by filtration onto 1.2 μm polycarbonate membrane filters (Millipore), flash frozen in liquid nitrogen, and then stored at −80°C for later analysis. Proteins were extracted and denatured in an extraction buffer (2% SDS, 10% glycerol, and 50 mmol L^{-1} Tris at pH 6.8; 1% β-mercaptoethanol was added after protein quantification) with heating at 100°C for 5 min. Insoluble material was pelleted by centrifugation at 16,000 $\times$ *g* for 10 min, and total protein in the supernatant was quantified using the bicinchoninic acid assay (Pierce, Thermo Scientific). For assay of NR protein, 6 μg of total protein from each sample was separated on a 12% SDS polyacrylamide gel for 100 min at 100 V in 1× SDS running buffer, and then transferred onto a PVDF membrane in ice-cold transfer buffer (25 mmol L^{-1} Tris, 192 mmol L^{-1} glycine and 2.5% methanol) for 1 h at 400 mA. For assay of PsbA, the D1 protein of PSII, 4 μg of total protein from each sample was separated on a 12% SDS polyacrylamide gel for 20 min at 80 V, followed by 40 min at 140 V in 1× SDS running buffer, and then transferred onto a PVDF membrane in ice-cold transfer buffer for 50 min at 400 mA. The membranes were then blocked for 1 h in TBST buffer (Tris-buffered saline with 0.25% Tween 20) containing 5% nonfat milk, followed by 1–2 h incubation with primary antibody (Agrisera Antibodies: NR, Art no. AS08 310; PsbA, Art no. AS05 084) and subsequently three 10-min washes with TBST buffer. The membrane was then probed with alkaline phosphatase-conjugated goat anti-rabbit IgG for 1 h, and washed three times again. Following three rinses with PhoA buffer (20 mmol L^{-1} Tris, 100 mmol L^{-1} NaCl, and 10 mmol L^{-1} $MgCl_2$, pH 9.5), protein bands on the membrane were visualized with NBT/BCIP (Roche) and quantified by densitometry. For quantification of PsbA, a standard curve obtained with the PsbA protein standard (Art no. AS01 016S, Agrisera Antibodies) was used to estimate the abundance of PsbA protein in experimental samples (Figure S1, Supporting Information).

RNA isolation and standard preparation

Total RNA was extracted from cultures using Trizol reagent (Invitrogen) according to the manufacturer's protocol. The extracted RNAs were treated with DNase (1 U, Promega) to eliminate genomic DNA contamination.

Standards for Quantitative Polymerase Chain Reaction (qPCR) were generated as follows. The cDNA was made by reverse-transcription of extracted RNA using mixtures of oligo $(dT)_{20}$ primer (5′-TTTTTTTTTTTTTTTTTTTT-3′) and random primer (5′-NNNNNN-3′) by M-MLV reverse transcriptase (BGI). The primer sequences of each gene were obtained from the literature (Table 2). The cDNA of approximately 150–450 bp were PCR amplified for each gene in 50 μL reactions containing approximately 5 μL cDNA template, 1.5 mmol L^{-1} $MgCl_2$, 0.4 mmol L^{-1} dNTPs, 400 nmol of each primer and 0.05 U Taq polymerase (Tiangen Biotech). The PCR reactions were carried out at 95°C for 3 min, followed by 29 cycles of 95°C for 15 s, 60°C for 30 s and 72°C for 30 s. Amplified products were separated by gel electrophoresis, purified and inserted into pMD 18-T vectors (Takara), and used to transform DH5α *Escherichia coli* competent cells. Plasmid DNA from positive clones was purified, quantified using UV1800 (Shimazu), and sequenced by Invitrogen Biotechnology.

Table 2. The PCR primers and genes used for qPCR.

Target gene	Primer sequence	Genbank ID	Fragment size (bp)	References
Nitrate reductase (NR)	F: TGAGGAAGCATAACAAGGAGG R: AGCATCAGAAACAACCGCCA	7453080	233	Parker and Armbrust 2005
Phosphoglycolate phosphatase (PGP)	F: TTGCCTGGTGTGGATGTC R: ATTTCTTCGGCGGGAACG	7451838	207	Parker and Armbrust 2005
T-protein subunit glycine decarboxylase (GDCT)	F: GGACCTGGTGCGGC R: CCAAGGTTGCTTCAATCGGA	7443516	322	Parker and Armbrust 2005
Sedoheptulose 1,7-bisphosphatase (SBP)	F: AGGAAACTGATGTTCTCCCTG R: GCGTGATACTTCCCAATGAG	7451690	317	Parker and Armbrust 2005
Carbonic anhydrase (CA)	F: ATGGCAACGGTCCTCATGGAAATGTTG R: AATGTCTTGTCCGCCAAGCGTAGTGAAA	7442183	308	McGinn and Morel 2008
Actin	F: ACTGGATTGGAGATGGATGG R: CAAAGCCGTAATCTCCTTCG	744941	162	McGinn and Morel 2008

Quantitative PCR

Genes that are representative of the Calvin cycle, photorespiration, CO_2 concentrating mechanism (CCM) and NO_3^- reduction were selected for analysis to quantify the changes of these metabolic pathways in response to changing growth conditions (Table 2). Sedoheptulose 1,7-bisphosphatase (SBP) is unique to the Calvin cycle, and its mRNA abundance reflects regulatory changes in carbon flux through this pathway (Parker and Armbrust 2005). Glycine decarboxylase T-protein (GDCT) and phosphoglycolate phosphatase (PGP) are both required for photorespiration. Carbonic anhydrases (CAs) are essential in the CCM and the CA gene analyzed here is a putative δ-CA in *T. pseudonana* (TpδCA3 in Samukawa et al. 2014). This gene's expression is negatively correlated with pCO_2 and the protein is localized to the periplastidal compartment, which suggests that it is involved in recovery of CO_2 leaking out of the chloroplast (McGinn and Morel 2008; Samukawa et al. 2014). NR is the essential enzyme for NO_3^- incorporation and often used as an index for NO_3^- uptake for diatoms (Berges and Harrison 1995a,b).

Total RNA was extracted, treated with DNase, and transcribed to cDNA as described above. All qPCR reactions were carried out on a fluorescent quantitative instrument CFX 96 TOUCH (Bio-Rad Laboratories). A SYBR Green I master mix (Zhishan Biotech) was used for qPCR in 15 μL reactions containing 3 μL of diluted cDNA, 0.4 mmol L^{-1} dNTPs, 200 nmol L^{-1} each of forward and reverse primers (Table 2) using the following thermal cycle program: 95°C for 3 min, followed by 40 cycles of 95°C for 10 s, 60°C for 25 s, and 70°C for 20 s. Standards corresponding to between 10^3 and 10^8 copies per well were amplified on the same 96-well plate as the cDNA generated from experimental materials. Dissociation curve analysis was done to confirm that only the targeted PCR product was amplified and detected. The RNA samples were also tested in a qPCR to make sure contaminating DNA was not present in the RNA extract (Parker and Armbrust 2005). To correct for differences in cDNA synthesis efficiency, the abundance of each transcript was normalized to the abundance of actin transcript (McGinn and Morel 2008).

Glycolic acid measurement

For measurements of extracellular glycolic acid, tripilicate 30-mL samples of cultures were syringe filtered through 0.22 μm membrane and the filtrate was acidified by adding concentrated HCl to the final concentration of 0.5 mol L^{-1}.^{13}C-glycolic acid (Sigma-Aldrich Chemical) was added as the internal standard to the final concentration of 20 ng L^{-1}. Extraction was performed by adding 5 mL HPLC grade ethyl acetate to a precombusted 40-mL borosilicate glass bottle (95 $\times$ 27.5 mm, C&W Technology). After vigorous shaking and phase separation, extraction of the aqueous fraction was repeated with another 5 mL ethyl acetate. The organic fractions were evaporated to dryness under N_2 stream and the residues were redissolved in 200 μL 0.01% formic acid.

A 2.1 $\times$ 150 mm Supelco Discovery® HS F5-3 column (particle size 3 μm, Sigma-Aldrich Chemical) was used for glycolic acid analysis, and the flow rate was 250 μL/min, which was delivered by an Agilent 1290 UPLC pump. The injection volume was 20 μL each time. The mobile phase consisted of two solvents: mobile phase A (0.01% formic acid) and mobile phase B (100% acetonitrile). The linear gradient program used for HPLC separation was as follows: hold isocratic at 0% B (0–6 min); linear gradient from 0% to 70% B (6–7 min); hold isocratic at 70% B (7–9 min). The effluent from the LC column was delivered to an Agilent 6490 triple-quadruple mass spectrometer, which was equipped with an electrospray ionization source operating in positive-ion mode. The concentration of glycolic acid was quantified using the isotope-dilution method using the ^{13}C-labeled glycolic acid as the internal standard. The selected MRM

transitions for the quantification of unlabeled and labeled glycolic acid were *m/z* 75 > 45 and 77 > 45, respectively. The MRM transition event of *m/z* 75 > 47 was also monitored simultaneously to verify the peak of glycolic acid.

Chlorophyll fluorescence

Samples with cell density of 3×10^5 mL^{-1} were dark adapted for 10 min to relax photosynthetic activity. Chlorophyll fluorescence characteristics of each sample were determined using a pulse amplified modulated (PAM) chlorophyll fluorometer (WATER-PAM Chlorophyll Fluorometer, Walz) with Win Control software. Minimum fluorescence (F_o) of the sample was measured with a weak probe pulse, and the maximum fluorescence (F_m) was then measured by applying a saturating light pulse of 4000 μmol photons m^{-2} s^{-1} for 0.8 s. Maximum quantum yield of PSII was estimated as $F_v/F_m = (F_m - F_o)/F_m$. Next the sample was illuminated with continuous actinic light adjusted to approximate the growth irradiance and fluorescence at ambient light (F) and maximal fluorescence in the presence of ambient light (F'_m). Photochemical quenching was calculated as $qP = 1 - (F - F'_o)/(F'_m - F'_o)$, and the capacity for heat dissipation through nonphotochemical quenching (NPQ) of fluorescence as $NPQ = F_m/F'_m - 1$.

A rapid light curve (RLC) was measured at nine different photosynthetic active radiation (PAR) levels (31 μmol photons m^{-2} s^{-1}, 154 μmol photons m^{-2} s^{-1}, 237 μmol photons m^{-2} s^{-1}, 349 μmol photons m^{-2} s^{-1}, 533 μmol photons m^{-2} s^{-1}, 796 μmol photons m^{-2} s^{-1}, 1129 μmol photons m^{-2} s^{-1}, 1579 μmol photons m^{-2} s^{-1}, and 2574 μmol photons m^{-2} s^{-1}) and each PAR lasted for 10 s, acquiring measurements for fluorescence and maximal fluorescence at each level to determine qP at each light level. The RLC was used to determine the light-limited photosynthetic rate (α), the relative electron transport rate (rETR = yield × PAR × 0.5 × 0.84, where the yield represents the effective quantum yield of PSII (i.e., $(F'_m - F)/F'_m$), the coefficient 0.5 takes into account that about 50% of all absorbed quanta reach PSII, and the parameter 0.84 corresponds to the faction of incident photons absorbed by photosynthetic pigments) at growth irradiance ($rETR_{LL\ or\ HL}$) and the maximal relative electron transport rate ($rETR_m$).

Short-term ^{15}N uptake

Subsample of 100 mL from each of the experimental cultures was poured into an acid-cleaned 125 mL polycarbonate bottle, followed by the addition of 100 μL 0.01 mol L^{-1} $Na^{15}NO_3$ and 100 μL 0.1 mmol L^{-1} $^{15}NH_4Cl$ to the NO_3^-- and NH_4^+-grown cultures, respectively. The bottles were then incubated for 1 h under the respective growth conditions in terms of light intensity. After the incubation cells were collected onto precombusted GF/F filters (Millipore) which were then washed with 0.22 μm-filtered oligotrophic seawater and stored at −80°C until analysis using IsoPrime 100 stable isotope mass spectrometry (Elementar). The background ^{15}N in the blank filters was < ~3% and < ~6%, respectively, yielding a final enrichment of ~0.39 atom % and ~0.36 atom %, respectively, of that in the NO_3^- and NH_4^+ experimental samples.

Energy budgets

A cellular energy budget was constructed for each growth condition based on energy generation from PSII, energy expenditures on carbon fixation, the CCM, NO_3^- reduction, and biochemical energy sinks in β-1,3-glucans, lipid, and proteins. Relative energy generation rates from PSII were calculated from cellular PSII content and relative ETR (as PsbA × rETR). As these rates are not absolute, a closed energy budget cannot be determined directly from them. Instead we made the assumption that energy was used fully and efficiently in the 400LLNO_3^- treatment, where energy demands were most severe and photosynthetic rates were lowest. All energy generation rates were normalized to relative rate in the 400LLNO_3^- treatment, and we then considered how changes in energy generation or expenditure relative to this condition would be predicted to affect net photosynthetic carbon fixation rates (Tables S2-S8, Supporting Information). These estimates assume that secondary energy expenditures (e.g., secondary metabolic pathways, frustule production, osmolyte synthesis, etc.) are constant across all growth conditions.

Statistical analysis

Data were analyzed using SPSS Statistics 19.0 (IBM Software) for significance of differences by two-way or multiple-way analysis of variance (ANOVA) combined with a LSD post hoc test. Significant differences in parameters among treatments were reported on tables and figures as different letters in superscription and same letter indicated insignificant difference. A significance level of $p < 0.05$ was applied, except as noted where significance was even greater.

Results

Growth and elemental composition

HL and NH_4^+ both stimulated the growth of *T. pseudonana* (Fig. 1a), and there were significant interactions between light and N source ($p < 0.001$, Table S1, Supporting Information). The growth rates of the NH_4^+-supplied cultures were 39–44% and 8.5–9.8% higher than the NO_3^--supplied cultures at LL and HL, respectively, and those of the HL cultures were 100–105% and 54–58% higher than the LL cultures when grown on NO_3^- and NH_4^+, respectively. Increase of pCO_2 from 400 μatm to 800 μatm, however, did not significantly change the growth rate (Fig. 1a).

The effects of a combination of light and N source on cellular C and N quotas were statistically significant ($p < 0.001$, Table S1, Supporting Information). In both NO_3^- and NH_4^+-supplied cultures, cellular C and N quotas, in general, were higher at HL than at LL; cells grown on NH_4^+ had higher cellular C and N content than those grown on NO_3^- (Figs.

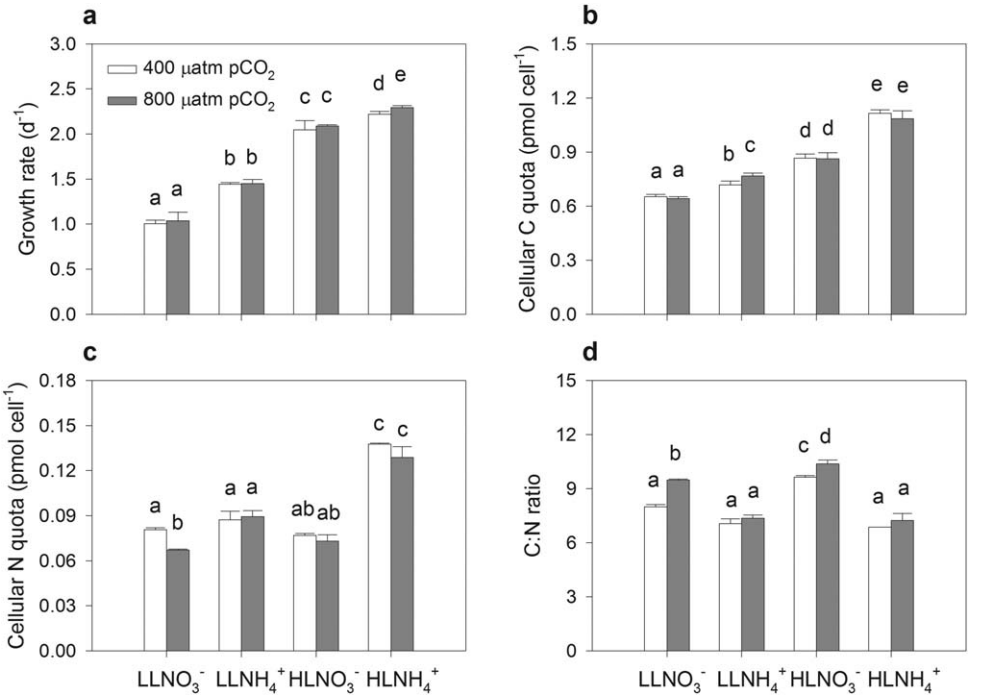

Fig. 1. The growth rate (a), cellular C quota (b) and N quota (c), and the C: N ratio (d) of the diatom *T. pseudonana* grown under eight conditions representing a matrix of light intensity (LL, 30 μmol photons $m^{-2}s^{-1}$; HL, 250 μmol photons m^{-2} s^{-1}), nitrogen source (100 μmol L^{-1} NO_3^- or NH_4^+), and pCO_2 (400 and 800 μatm). The data are mean + SD ($n = 3$). Different letters in superscription indicate significant differences ($p < 0.05$) among treatments (multiple-way ANOVA followed by LSD post hoc tests).

1b,c). Cellular C quotas in *T. pseudonana* cells did not show noticeable response to elevated pCO_2 (Fig. 1b). However, there were significant interactive effects between light, N source and CO_2 on cellular N quotas ($p = 0.028$, Table S1, Supporting Information). For NO_3^--supplied cultures, an increase in pCO_2 from 400 μatm to 800 μatm resulted in 17% and 5% lower cellular N content at LL and HL, respectively; while for NH_4^+-supplied cultures, the effect on cellular N content of elevated pCO_2 was not consistent (Fig. 1c).

Particulate C: N ratios were greater in NO_3^--grown cells than in NH_4^+-grown cells (Fig. 1d), particularly at HL, which were mainly caused by smaller nitrogen quotas in NO_3^--grown cells. Increase of pCO_2 from 400 μatm to 800 μatm resulted in significantly higher C: N ratios in NO_3^--supplied cultures ($p = 0.007$; Fig. 1d), which were mainly due to the smaller cellular N quotas for cells grown at 800 μatm pCO_2. For NH_4^+-supplied cultures, the slightly but not significantly greater C: N ratios at higher pCO_2 were the results of the combined effects on the changes in cellular C and N quotas.

Steady-state net N and C uptake

The steady-state net uptake rates of N and C were calculated as growth rate (d^{-1}) times cellular N or C quotas (pmol $cell^{-1}$). The results showed that HL and NH_4^+ both significantly increased steady-state net N and C uptake rates among most treatments ($p < 0.001$; Fig. 2a,b). In NO_3^--supplied cultures, increased pCO_2 reduced the steady-state net N uptake rate (Fig. 2b), which was confirmed by short-term $^{15}NO_3^-$ uptake experiments (Fig. 2c). In addition, these results were in agreement with the lower cellular N quotas in high CO_2 cells grown on NO_3^- (Fig. 1c). Consistently, in the same cultures both the activity and expression of NR, which is the essential enzyme for N incorporation (Berges and Harrison 1995a), were lower in high CO_2 treated cells (Fig. 3).

Biochemical composition

Protein content of *T. pseudonana* cells (Fig. 4a) had good correlation with the particulate organic nitrogen (PON) and on average it made up 82% of total cellular N (Fig. 1c), suggesting that protein was the major sink of assimilated nitrogen for both NO_3^-- and NH_4^+-supplied cells. The cellular contents of fatty acids and β-1,3-glucan (Fig. 4b,c), two major storage reservoirs of photosynthetic fixed carbon and sinks for energy and reductants, were both affected significantly by light ($p < 0.001$) and by the interactions between light and N source ($p = 0.008$ and 0.014 for fatty acids and β-1,3-glucan, respectively, Table S1, Supporting Information). They were higher in HL cells than in LL cells ($p < 0.001$), and NH_4^+-grown cells had higher fatty acids content but lower β-1,3-glucan content than NO_3^--grown cells, which decreased β-1,3-glucan: fatty acids ratios in the range of 27–39%. Increasing pCO_2 from 400 μatm to 800 μatm resulted in an

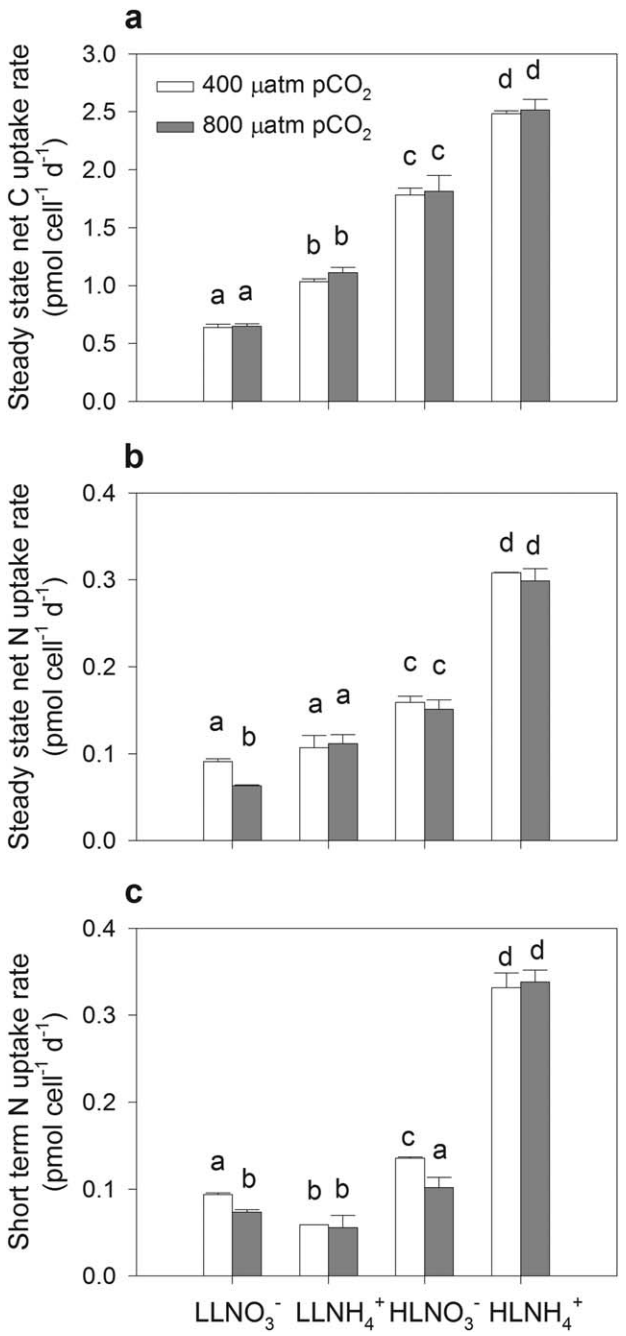

Fig. 2. The steady-state net C (a) and N (b) uptake and the short-term N uptake (c) of the diatom *T. pseudonana* grown under eight conditions as described in Fig. 1. The data are mean + SD ($n = 3$). Different letters in superscription indicate significant differences ($p < 0.05$) among treatments (multiple-way ANOVA followed by LSD post hoc tests).

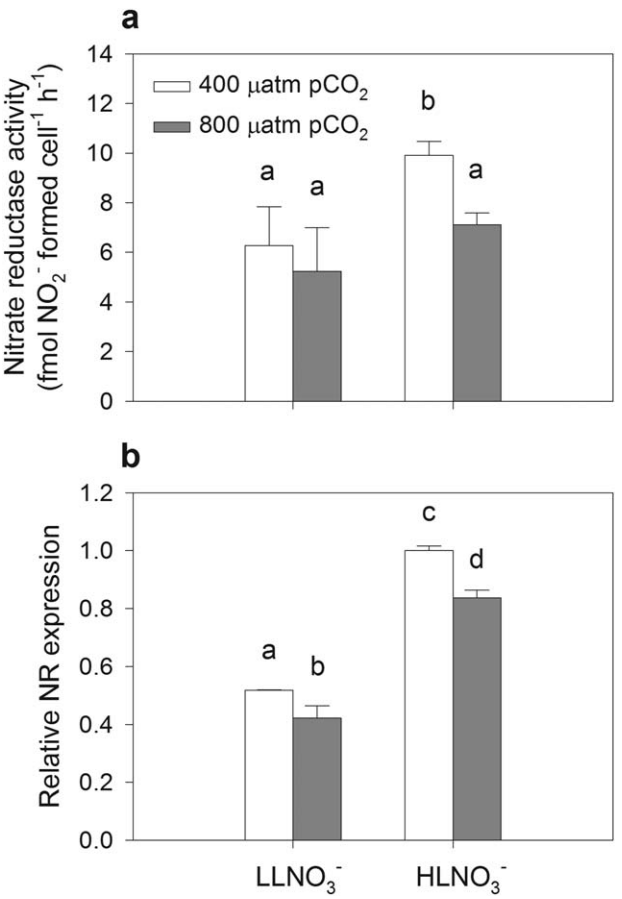

Fig. 3. The activity (a) and protein expression (b) of NR in the diatom *T. pseudonana* grown under four conditions, as described in Fig. 1, with 100 μmol L^{-1} NO_3^- as the sole added nitrogen source. The data are mean + SD ($n = 3$). Different letters in superscription indicate significant differences ($p < 0.05$) among treatments (two-way ANOVA followed by LSD post hoc tests).

increase in β-1,3-glucan and fatty acid content by 3–29% and 4–10%, respectively.

Gene transcription levels and glycolic acid excretion

Because actin mRNA copy number had good correlation with total extracted RNA across all experimental treatments (i.e., irradiance, N source and CO_2; data not shown), actin mRNA was used to normalize mRNA copy numbers of NR, CA, SBP, GDCT, and PGP genes to account for variations in RNA extraction and reverse-transcription (Figs. 5, 6). NR mRNA expression was about 10 fold lower in NH_4^+-grown cells than in NO_3^--grown cells (Fig. 5a). In NO_3^--supplied cultures, transcript abundances of the NR gene decreased at high pCO_2. Even though the decrease was insignificant ($p = 0.052$), it was consistent with decreases in NR activity and NR protein expression at high pCO_2 (Fig. 3). Transcript abundances of a CA gene, which is part of the CCM, decreased significantly at higher pCO_2 ($p = 0.043$; Fig. 5b).

SBP was chosen to represent the Calvin cycle and PGP and GDCT were chosen to represent photorespiration, the two major pathways for carbon metabolism. The transcript abundance of SBP, PGP, and GDCT genes were lower at LL than at HL and no significant difference was detected among different treatments at LL (data not shown). At HL, the mRNA copy ratios of SBP/actin, PGP/actin, and GDCT/actin

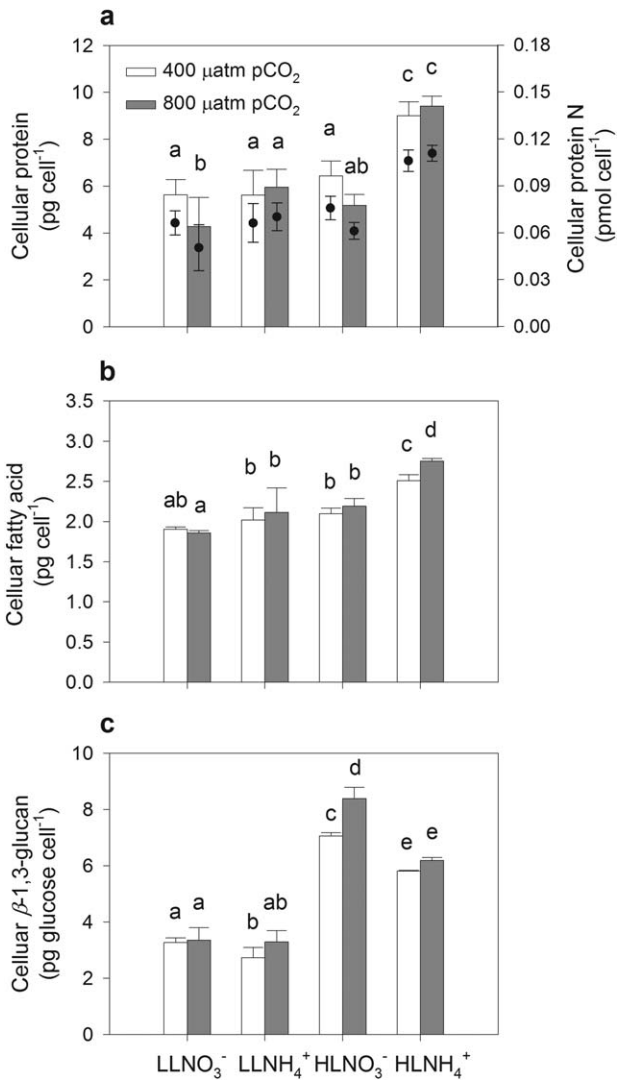

Fig. 4. The cellular content of protein (bars) and protein N (circles; a), fatty acids (b), and β-1,3-glucan (c) in the diatom *T. pseudonana* grown under eight conditions as described in Fig. 1. The data are mean + SD ($n = 3$). Different letters in superscription indicate significant differences ($p < 0.05$) among treatments (multiple-way ANOVA followed by LSD post hoc tests).

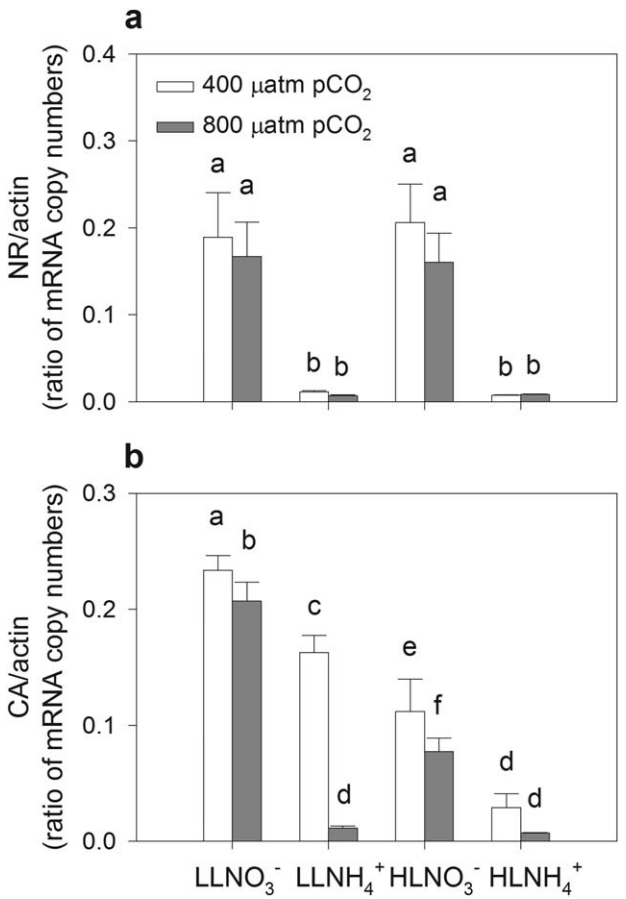

Fig. 5. Ratios of copy numbers of NR (a) and CA mRNA (b) to actin mRNA in the diatom *T. pseudonana* grown under eight conditions as described in Fig. 1. The data are mean + SD ($n = 3$). Different letters in superscription indicate significant differences ($p < 0.05$) among treatments (multiple-way ANOVA followed by LSD post hoc tests).

were all greater in NH_4^+ grown cells (Fig. 6a,c), suggesting the upregulation of both C fixation through the Calvin cycle and photorespiration in cells grown on NH_4^+. In NO_3^--supplied cultures, cells treated with high CO_2 had lower PGP/actin and GDCT/actin ratios than low CO_2 treatments (Fig. 6b,c), suggesting reduced rates of photorespiration at elevated pCO_2. Consistent with this, the concentration of glycolic acid excreted by high CO_2 cells was much lower than low CO_2 cells, further confirming the reduction of photorespiration by elevated pCO_2 (Fig. 6d).

Chlorophyll fluorescence

F_v/F_m was high in all treatments with the only difference among treatments being a slight depression in the HL, NO_3^- supplied cells (Table 3). qP at growth irradiance was significantly lower under HL conditions ($p < 0.001$), and was also lower when cells were grown on NH_4^+ at HL. NPQ was minimal under LL but increased to modest levels at HL. NPQ was slightly reduced by elevated pCO_2, but not consistently altered by the other factors. $rETR_m$ was fairly constant among treatments, but there were some statistically significant differences including a reduction when grown on NH_4^+ at high light ($p = 0.028$) and a reduction when grown at high CO_2 under low light ($p = 0.022$), showing significant interactions both between light and N source and between light and CO_2 ($p < 0.001$, Table S1, Supporting Information). rETR at growth irradiance (LL or HL) was strongly affected by the ambient irradiance, but was otherwise unaffected by the treatments except for a small decline when grown on NH_4^+ at HL.

PsbA protein expression

The expression of PsbA, the core subunit of PSII, was significantly upregulated by switching nitrogen source from NO_3^- to NH_4^+ by approximately 50% and 100%, respectively,

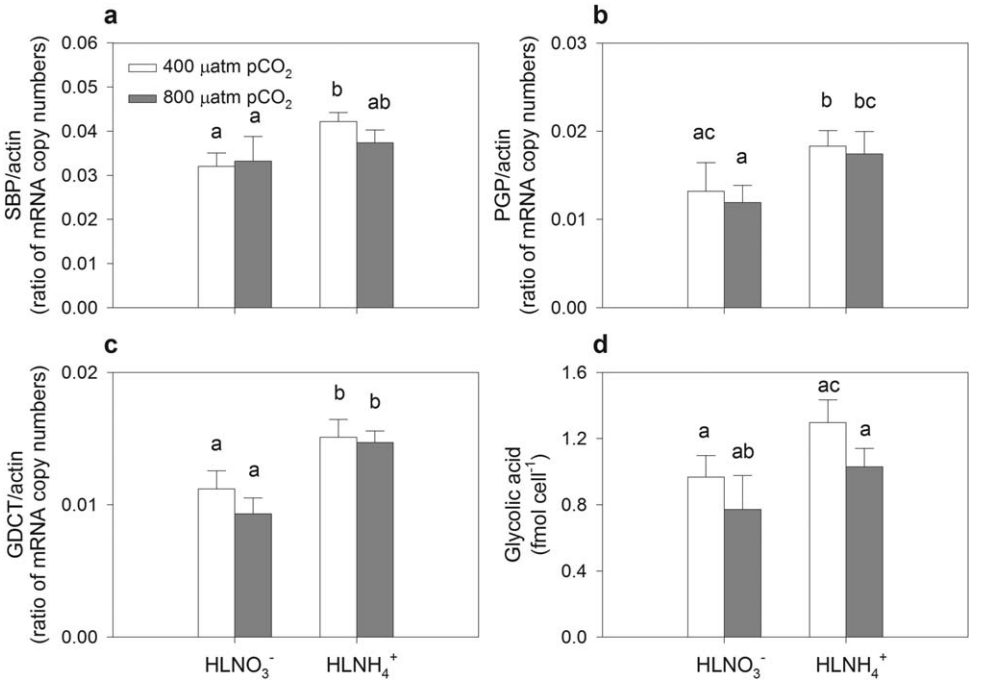

Fig. 6. Ratios of copy numbers of SBP (a), PGP (b), and GDCT (c) mRNA to actin mRNA, and the excretion of glycolic acids (d) in the diatom *T. pseudonana* grown under four conditions, as described in Fig. 1, at high light (250 μmol photons m^{-2} s^{-1}). The data are mean + SD ($n = 3$). Different letters in superscription indicate significant differences ($p < 0.05$) among treatments (two-way ANOVA followed by LSD post hoc tests).

Table 3. Photochemical quantum yield of photosystem II (F_v/F_m), photochemical quenching (qP), NPQ, the maximal rate of relative electron transport at the saturating irradiance (rETRm), and relative electron transport rate at the growth irradiance ($rETR_{LL\ or\ HL}$) of the diatom *T. pseudonana* grown under eight conditions representing a matrix of light intensity (LL, 30 μmol photons m^{-2} s^{-1}; HL, 250 μmol photons m^{-2} s^{-1}), nitrogen source (100 μmol L^{-1} NO_3^- or NH_4^+), and pCO_2 (400 and 800 μatm). The data are mean ± SD ($n = 3$). Different letters in superscription indicate significant differences ($p < 0.05$) among treatments (multiple-way ANOVA followed by LSD post hoc tests).

Treatment	F_v/F_m	qP	NPQ	rETRm	$rETR_{LL\ or\ HL}$
LL400NO_3^-	0.69 ± 0.00^{a}	0.91 ± 0.01^{a}	0.05 ± 0.01^{a}	146.2 ± 0.6^{ac}	8.7 ± 0.5^{a}
LL800NO_3^-	0.68 ± 0.00^{a}	0.90 ± 0.01^{a}	0.04 ± 0.02^{a}	123.3 ± 5.4^{bd}	8.6 ± 0.2^{a}
LL400NH_4^+	0.70 ± 0.01^{a}	0.89 ± 0.02^{a}	0.07 ± 0.01^{a}	141.8 ± 3.0^{a}	8.9 ± 0.6^{a}
LL800NH_4^+	0.69 ± 0.01^{a}	0.90 ± 0.00^{a}	0.04 ± 0.01^{a}	122.1 ± 3.2^{bd}	8.8 ± 0.4^{a}
HL400NO_3^-	0.67 ± 0.01^{ab}	0.72 ± 0.03^{b}	0.18 ± 0.06^{b}	133.0 ± 19.1^{ad}	47.9 ± 2.9^{b}
HL800NO_3^-	0.66 ± 0.00^{b}	0.75 ± 0.01^{b}	0.12 ± 0.04^{b}	158.0 ± 7.4^{c}	47.8 ± 1.2^{b}
HL400NH_4^+	0.70 ± 0.02^{a}	0.63 ± 0.02^{c}	0.29 ± 0.05^{c}	103.9 ± 3.2^{d}	42.4 ± 3.4^{c}
HL800NH_4^+	0.69 ± 0.01^{a}	0.68 ± 0.01^{d}	0.20 ± 0.03^{b}	116.3 ± 5.5^{d}	44.3 ± 4.7^{bc}

under LL and HL conditions ($p < 0.001$; Fig. 7). Compared with LL, *T. pseudonana* cells expressed slightly but significantly less PsbA at HL ($p = 0.036$). Change of pCO_2 generally did not have effects on the expression of PsbA protein.

Discussion

Energetic balance under differing environmental conditions

In marine phytoplankton light energy is captured and converted to chemical energy in the light reactions of photosynthesis and is then used primarily for carbon fixation via the Calvin cycle, but also for other metabolic processes including reduction of NO_3^-, powering the CCM, and dealing with photorespiration. We developed an energy budget for *T. pseudonana* that considers energy generation in the photosystems and the major energy expenditures listed above, which were expected to be altered by the experimental treatments. The energetics of the Calvin cycle are well-understood [590 kJ $(mol\ C)^{-1}$ fixed] and invariant among phytoplankton (Table 4). Similarly, the reduction of NO_3^- uses a common pathway, which requires 288 kJ per mole

NO_3^- reduced (Falkowski and Raven 2007). In contrast, the CCM, which raises the CO_2 concentration around RubisCO to increase its efficiency, differs among phytoplankton taxa. These systems are not as well-understood, but the CCM has been reasonably well-studied in diatoms, where it is estimated to use ~ 75–300 kJ (mol C)$^{-1}$ fixed (Hopkinson et al. 2011). Photorespiration is primarily an undesired by-product of using RubisCO, but it may also serve to dissipate excess light energy especially under high light conditions (Beardall 1989; Parker et al. 2004; Parker and Armbrust 2005). The rates of photorespiration in diatoms appear to be modest under most conditions, but it is energetically expensive requiring 872 kJ (mol C)$^{-1}$ (Table 4). Without the function of enzymes, such as GDC downstream in the photorespiratory pathway to recover the carbon from glycolate, photorespiration would also result in the release of dissolved organic carbon (DOC) such as glycolate (Parker et al. 2004) as well as

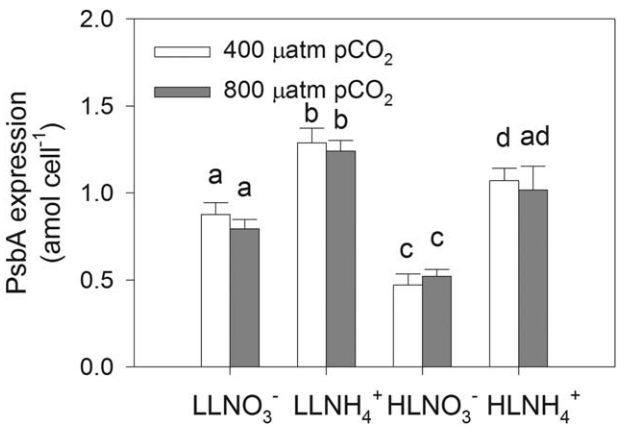

Fig. 7. Expression of PsbA protein in the diatom *T. pseudonana* grown under eight conditions as described in Fig. 1. The data are mean + SD ($n = 3$). Different letters in superscription indicate significant differences ($p < 0.05$) among treatments (multiple-way ANOVA followed by LSD post hoc tests).

CO_2 and ammonia (NH_3) (Lomas et al. 2000; Wingler et al. 2000). The ultimate energy sinks for captured light energy are mainly carbohydrates, proteins, and lipids, among which lipids have higher energy densities than proteins and carbohydrate (Table 4).

In the present study, we used the diatom *T. pseudonana* as a model organism to study how phytoplankton adjust their metabolism to balance the cellular energy budget in response to changes in environmental factors such as irradiance, nitrogen source, and CO_2. Under the conditions tested, nitrogen source and irradiance had dramatic effects on biogeochemically relevant variables such as growth and photosynthesis, while CO_2 had more modest effects (Figs. 1, 2, 8). Comparing the responses observed with predictions based on energetic budgets showed that the energetic budgets offered significant insight into the responses observed, and did a reasonable job predicting those responses.

A shift in nitrogen source from NO_3^- to NH_4^+ resulted in a ~ 60% increase in net photosynthesis at LL and a 40% higher photosynthetic rate at HL (Fig. 2a; "Relative observed photosynthetic rate," Table 5). However, the energy saved from not needing to reduce NO_3^- was only predicted to allow a 1.5–4% increase in photosynthetic rates under both LL and HL (Table 5). Instead, the primary effect of the shift to NH_4^+ was to allow synthesis of more photosynthetic complexes, as indicated by PsbA content (Figs. 7, 8), which increased light capture and energy generation. The photosynthetic systems contain a significant portion (15–25%) of total cellular nitrogen (Li et al. 2014), and so presumably the lower costs of NH_4^+ incorporation relative to NO_3^- makes it worthwhile to create more photosynthetic complexes when NH_4^+ is available. Incorporating this increased energy production and secondary energetic expenditures (NR, CCM, and photorespiration) into the energy budget led to the prediction that photosynthesis should increase by ~ 50% at LL and by ~ 90% at HL (Table 5). The predictions and observations ("Relative predicted photosynthetic rate" vs. "Relative

Table 4. Theoretical energy costs for different metabolic processes involved in the metabolism of harvested light energy.

	ATP and NADPH (per C or N)	kJ (mol C)$^{-1}$	References
Calvin cycle	3 ATP and 2 NADPH	590*	Raven et al. 2000
CCM	1.5–6 ATP	75–300*	Hopkinson et al. 2011
NO_3^- reduction to NH_4^+		43†	Falkowski and Raven 2007
Photorespiration carbon cycle	4.25 ATP and 3 NADPH‡	872*	Raven et al. 2000
Biochemical energy sinks			
Carbohydrates		605	Norici et al. 2011
Proteins		883	
Lipids		945	

*Calculated based on the free energy of ATP hydrolysis and NADPH oxidation (50 kJ mol^{-1} and 220 kJ mol^{-1}, respectively) (Subramanian et al. 2013).
†The reduction of NO_3^- to NH_4^+ requires 288 kJ per mole NH_4^+ formed (Falkowski and Raven 2007), and for a Redfield C: N ratio of 6.6 requires 43 kJ (mol C)$^{-1}$.
‡The values are for the glycolate oxidase variant of the photorespiration carbon cycle (Raven et al. 2000).

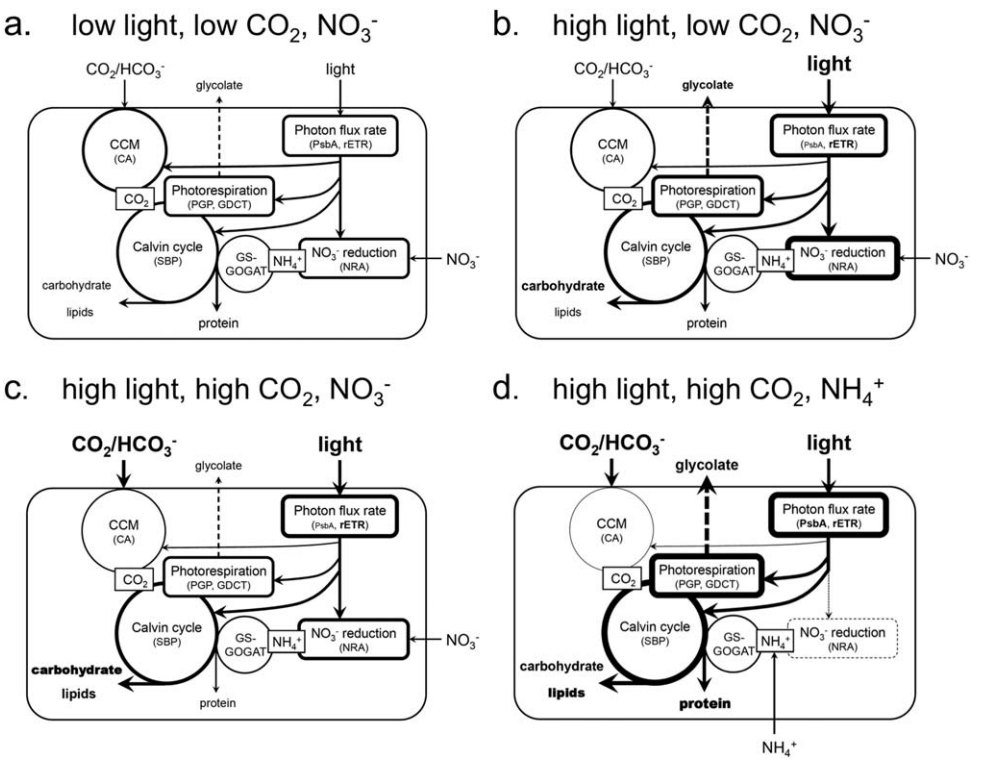

Fig. 8. A conceptual model of the diatom *T. pesudonana* showing photosynthetic energy generation (calculated as PsbA × rETR), major cellular energy expenditures (CCM, the Calvin cycle, photorespiration, and NO_3^- reduction), and ultimate energy sinks (carbohydrate, lipids, and protein) in response to four representative growth conditions: (a) low light, low CO_2, and NO_3^-; (b) high light, low CO_2, and NO_3^-; (c) high light, high CO_2, and NO_3^-; and (d) high light, high CO_2, and NH_4^+. Increased/decreased thickness of lines and size of arrow and font indicate increased/decreased use of the pathway.

observed photosynthetic rate," Table 5) at LL, when energy is clearly limiting, are in very good agreement, but the energetic budget over-predicts the response to NH_4^+ at high light.

One possible explanation for the discrepancy at HL is that excess energy is put into higher energy biochemical sinks. When light is in excess, lipids and protein can serve as more energy-dense sinks than carbohydrate (Table 4). At HL, switching from NO_3^- to NH_4^+ resulted in about 40–80% increase in cellular protein content, which was much more significant than cells at LL (Figs. 4a, 8). Additionally, $HLNH_4^+$-grown cells produced markedly more fatty acid (~ 25% more) but less β-1,3-glucan (~ 30% less), compared to $HLNO_3^-$-grown cells (Figs. 4b,c, 8). A similar shift of C storage from carbohydrate to energy-dense lipid was found when the diatom *Skeletonema marinoi* was grown at high light (Norici et al. 2011), and the quantum requirements for fatty acid synthesis in the diatom *Phaeodactylum tricornutum* were reduced when shifted from NO_3^- to NH_4^+, suggesting that in the absence of energetically demanding NO_3^- assimilation cells opt to store additional energy (Frada et al. 2013). Taking into account the extra energy captured in the forms of protein and lipids reduces the photosynthetic rate at $HLNH_4^+$ by ~ 10% (Table 5), but there is still a large discrepancy between the predicted and observed photosynthetic rates at $HLNH_4^+$ ("Relative predicted photosynthetic rate" vs. "Relative observed photosynthetic rate," Table 5). This could be because under optimal growing conditions, such as those experienced in the $HLNH_4^+$ treatments, the rate of photosynthesis is often limited by Calvin cycle kinetics rather than energy generation from the photosystems (Sukenik et al. 1987). Consistent with this, there is an increase in NPQ at HL when growing on NH_4^+ compared togrowth on NO_3^- (Table 3), indicating that energy generation in the photosystems exceeds capacity of downstream metabolism.

Rather than an underestimation of the energy sinks, the energy budget may overestimate energy generation rates under $HLNH_4^+$ growth conditions. Per cell energy generation rates were estimated by multiplying the rETR through each PSII unit ($rETR_{LL\ or\ HL}$) by the moles of PSII per cell (using PsbA protein content as a proxy for PSII content). However, several recent studies have shown that a significant fraction of PsbA is in inactive PSII units in *T. pseudonana* (Wu et al. 2011; Campbell et al. 2013; Li and Campbell 2013). *T. pseudonana* maintained a similar fraction of PsbA in an inactive state across a wide range of growth light levels (38–380 μmol photons m^{-2} s^{-1}; Campbell et al. 2013), so changes in light alone are not likely to have biased the energy generation estimates. The effects of nitrogen source on the fraction of

Table 5. Energy balance in the diatom *T. pseudonana* cells grown under eight conditions as described in Table 3.

	LL				HL			
	$400NO_3^-$	$800NO_3^-$	$400NH_4^+$	$800NH_4^+$	$400NO_3^-$	$800NO_3^-$	$400NH_4^+$	$800NH_4^+$
Relative photon flux rate*	1	0.90	1.50	1.43	2.96	3.27	5.96	5.92
Potential C fixation rate by change of photon flux (pmol cell^{-1} d^{-1})†	0.64	0.58	0.97	0.92	1.89	2.09	3.81	3.79
Contribution to photosynthetic rate by downregulation of CCM (pmol cell^{-1} d^{-1})‡	—	0.04	—	0.07	—	0.12	—	0.17
Contribution to photosynthetic rate by increase/decrease of NO_3^- reduction relative to LL400NO_3^- (pmol cell^{-1} d^{-1})§	—	0.014	0.044	0.044	−0.034	−0.029	0.044	0.044
Contribution to photosynthetic rate by upregulation/downregulation of photorespiration (pmol cell^{-1} d^{-1})‖	—	—	—	—	−0.18	−0.16	−0.25	−0.24
Contribution to photosynthetic rate by changes in biochemical energy sinks (protein/β-1,3-glucan/lipids) relative to LL400NO_3^- (pmol cell^{-1} d^{-1})¶	—	0.02	−0.09	−0.10	−0.26	−0.24	−0.45	−0.52
Predicted photosynthetic rate (pmol cell^{-1} d^{-1})#	0.64	0.66 (0.63)	0.92 (1.01)	0.93 (1.03)	1.42 (1.68)	1.79 (2.03)	3.16 (3.61)	3.25 (3.76)
Relative predicted photosynthetic rate**	1	1.03 (1.00)	1.43 (1.58)	1.45 (1.61)	2.21 (2.62)	2.80 (3.17)	4.93 (5.64)	5.07 (5.88)
Relative observed photosynthetic rate††	1	1.01	1.62	1.73	2.79	2.83	3.88	3.93

*Relative photon flux rate was calculated as $rETR_{LL \text{ or } HL} \times$ PsbA, which then was normalized to the LL400NO_3^- group (Table S3, Supporting Information).

†Potential C fixation rate by change of photon flux was calculated as relative photon flux rate × steady state net C uptake rate at LL400NO_3^-, which was 0.64 pmol cell^{-1} d^{-1} (Fig. 2a).

‡Table S4 (Supporting Information).

§Table S5 (Supporting Information).

¶Table S6 (Supporting Information). The photorespiration at LL was low and there was no significant difference in the expression of either GDCT or PGP genes. Thus, the contribution of photorespiration to photosynthesis was not included in the calculation for LL conditions.

‖Tables S7 and S8 (Supporting Information).

#Predicted photosynthetic rate was the sum of potential C fixation rate by change of photon flux, contribution to photosynthetic rate by upregulation/downregulation of CCM, NO_3^- reduction, photorespiration, and changes in biochemical energy sinks. The values in parenthesis were predicted without taking into account changes in biochemical energy sinks.

**Relative predicted photosynthetic rate was calculated by normalization of predicted photosynthetic rate to the LL400NO_3^- group. The values in parenthesis were predicted without taking into account changes in biochemical energy sinks.

††Relative observed photosynthetic rate was calculated based on steady-state net C uptake rate in Fig. 2a.

inactive PsbA have not yet been evaluated, but it is conceivable that more inactive PsbA may be allowed to accumulate when grown on NH_4^+ as it is energetically cheaper to assimilate than NO_3^-. A greater fraction of inactive PsbA when grown on NH_4^+ would lead to an overestimate of energy generation. It should also be noted that cells grown on different nitrogen sources may exhibit distinct nitrogen flows. For instance, NH_4^+-grown *T. pseudonana* cells have remarkably lower transcription levels of gene involved in the urea cycle, glutamine synthesis and pyrimidine synthesis, particularly under HL, and thus would probably affect the cellular energy budget as well (Parker and Armbrust 2005; Bender et al. 2012).

The primary effect of increasing the light intensity was to increase the photosynthetic electron transport rate leading to increased growth rates. Despite slight declines in PSII content at HL, the photosynthetic electron transport rate increased as a result of large increases in the rETR per PSII unit (Fig. 8). Much of this increased energy generation went to production of new biomass to promote growth as indicated by higher CO_2 and N assimilation rates and increased growth rates, but some was put toward energy storage,

primarily in the form of β-1,3-glucans (Fig. 8). When growing on NO_3^- the cellular energy budget did a remarkably good job predicting the effect of increased light on net photosynthesis, but when growing on NH_4^+ there were discrepancies as discussed previously.

The effects of CO_2 on photosynthesis and growth were negligible to modest under all conditions (Fig. 8). The increase in pCO_2 did not significantly affect the photon flux rate through the PSII or PSII content, the factors that had the largest consequences for changes in growth and photosynthesis when light and N-source were varied. It has been estimated that doubling of ambient pCO_2 would save about 20% of CCM energy expenditure, decreasing the energy requirement for C fixation by 15–60 kJ (mol C)$^{-1}$ (Hopkinson et al. 2011). Here, we showed that in *T. pseudonana* the expression of a δ-CA, a component of the CCM, was significantly downregulated by CO_2 enrichment, consistent with CCM downregulation at high CO_2. Using the energy savings estimated in Hopkinson et al. (2011) implies that carbon fixation rates could increase by only 2.5–10%, and the observations are on the lower end of this range with no significant effect of CO_2 on net photosynthesis (Fig. 2a).

Although the effect of CO_2 on photorespiration in marine phytoplankton has not been thoroughly examined, it has been suggested in terrestrial C3 plants that elevated pCO_2 could increase the CO_2/O_2 ratio, promote RubisCO carboxylation, and thus result in lower photorespiration (Koch et al. 2013). CO_2 enrichment led to downregulation of photorespiration in the diatom, as indicated by the lowered transcription of GDCT and PGP genes and the reduced excretion of glycolic acid in NO_3^--grown cells at high CO_2 (Figs. 6, 8), consistent with previous reports on gene expression in *T. pseudonana* (Roberts et al. 2007). However, in an outdoor experiment on *T. pseudonana* conducted under solar exposure, Gao et al. (2012) observed increases in photorespiration at high CO_2. Using the RubisCO kinetic properties of the diatom *P. tricornutum* (Badger et al. 1998) and estimated concentrations of CO_2 (60 μmol L^{-1}; Hopkinson et al. 2011) and O_2 (218 μmol L^{-1}, in air-equilibrated seawater at 20°C and salinity = 35; Garcia and Gordon 1992) around RubisCO, photorespiration rates in diatom were estimated to be $\sim$ 7% of carbon fixation rates (Table S2, Supporting Information). If these rates decline by 15% at high CO_2 (as suggested by the downregulation of GDCT and PGP, Fig. 6b,c), the energetic savings could promote increased photosynthetic rates of $<$ 2% at high CO_2 (Table 5). Again, net photosynthetic rates and growth rates of *T. pseudonana* are largely unaffected by CO_2 (Figs. 1a, 2a), consistent with the small estimated energetic benefits from reduced CCM function and photorespiration. Using the same rationale, the extra energy expended on photorespiration at HL condition could reduce photosynthetic rates by $\sim$ 4% in NH_4^+-grown cells compared to NO_3^- grown cells (Table 5). Although the effects of CO_2 on photosynthesis and growth were small in this study, this does not necessarily mean that it is the least relevant of the global change variables assessed here. Predictions for future oceanic CO_2 concentrations are well-constrained, but predictions for changes in light intensity and N-source shifts are more uncertain. In this study, large shifts in light intensity and a complete switch from NO_3^- to NH_4^+ were used to encompass a wide range of future scenarios and elicit strong responses, but these dramatic changes may not occur in the future ocean.

As the ocean evolves into an unprecedented state due to anthropogenic activities, marine phytoplankton dwelling in surface waters will likely encounter enhanced irradiance, more reduced nitrogen and increased water acidity simultaneously. One approach to predicting how phytoplankton will respond to these coupled changes is to use cellular energy budgets, an approach we tested here on the diatom *T. pseudonana*. For *T. pseudonana*, changes in light capture and processing through the photosystems induced by changes in environmental conditions had by far the strongest effect on growth and photosynthesis. In comparison, changes in energetic expenditures were secondary considerations. The energetic budgets did a good job predicting the effects of changing conditions on photosynthesis and growth under LL when energy is strongly limiting, but were less accurate at HL. These results suggest that energetic considerations may be used, with appropriate caution, to help predict the effects of global change on marine primary productivity (Allen et al. 2005; Lopez-Urrutia et al. 2006).

The use of energetic budgets may be especially helpful for refining predictions about the biological responses to global change as our understanding of the forcing factors become more precise. For example, although we currently have a good handle on expected future oceanic CO_2 concentrations, the future light environment and relative availability of NH_4^+ and NO_3^- are less well-understood. However, having shown that the effects of these variables can be reasonably accounted for using an energetic budget, predictions about the response of *T. pseudonana* and similar diatoms to global change can be updated as the driving variables (light, N-source) are better constrained.

Effect of CO_2 on nitrogen metabolism

The effects of changing pCO_2 on nitrogen acquisition and assimilation by marine algae are largely unknown. Limited studies show that the effects of rising CO_2 on the utilization of NO_3^- seem to vary in different algal species. For instance, the N quotas of the coccolithophore *E. huxleyi* in nutrient-replete cultures positively correlated with CO_2 in the range of $\sim$ 500 ppm to 1100 ppm, as did its NR activity (Rouco et al. 2013). In contrast, NR activity of the green algae *Chlamydomonas reinhardtii* and *Chlorella pyrenoidosa* decreased on CO_2 enrichment (Xia and Gao 2005). In the seagrass *Zostera noltii* and rhodophyte *Corallina officinalis*, which were exposed to varying pCO_2 for months in mesocosms, NO_3^-

uptake rates were inversely related to pCO_2 (Alexandre et al. 2012; Hofmann et al. 2013). Interestingly, several studies on terrestrial plants have reported that increasing pCO_2 could suppress NO_3^- uptake and assimilation in C3 plants and thus result in lower protein content (Myers et al. 2014; Bloom 2015).

In the present study, we found that elevated pCO_2 strikingly reduced NO_3^- uptake in *T. pseudonana* at both HL and LL, as indicated by both short-term and steady-state net NO_3^- uptake rates (Fig. 2b,c). This impaired utilization of NO_3^- was further supported by the reduced gene transcription, protein expression and enzymatic activity of NR at high CO_2 (Figs. 3, 5). The diminished NO_3^- uptake at elevated pCO_2 resulted in lower PON and total protein content, consequently increasing the C: N ratios. Consistent with our results, Hennon et al. (2014) cultured *T. pseudonana* in a NO_3^--limited chemostat for 15–18 generations and observed decreasing DIN uptake at high CO_2, which led to an increased DIC: DIN drawdown ratio. It has also been reported that N quotas in *T. pseudonana* declined slowly as CO_2 increased from 380 ppm to 1500 ppm in non-nutrient limited cultures (Reinfelder 2012). Although the underlying mechanisms of the downregulation of NO_3^- uptake and assimilation by elevated pCO_2 remain to be elucidated, our study demonstrates that seawater acidification may have important effects on marine primary producers, not only through the direct effects on carbon fixation as reported by many studies (e.g., Riebesell et al. 2007; Tortell et al. 2008), but also through the indirect effects on nitrogen utilization. It should also be noted that the concurrently warming effect caused by rising CO_2 could further suppress NO_3^- reduction due to the inverse temperature dependency of NR (Lomas and Glibert 1999). As NO_3^- is one of the primary nitrogenous nutrients supporting oceanic primary production, any interference in its utilization by marine phytoplankton would lead to an enormous impact on the biogeochemical cycles of carbon and nitrogen in marine ecosystems.

Relevance to marine food webs

Several of the responses to changing environmental conditions observed in *T. pseudonana* have important implications for how energy and materials are routed through pelagic ecosystems. Glycolic acid is one of the major components of organic acids released by diatoms and contributes to a significant portion of DOC in seawaters (Leboulanger et al. 1997). It is rapidly taken up by heterotrophic microorganisms living in the planktonic communities and appears to serve as an energy source for the growth of marine bacteria (Fogg 1983). Hence, the increasing supplies of light and CO_2 and chemically reduced nitrogen may exert an effect on the seawater DOC and the microbial-mediated marine carbon cycle.

The C:N stoichiometry of phytoplankton is one of the most influential factors controlling the strength of the biological pump (Broecker 1982). Shifting of the C:N ratios may change the nutritional value of the particulate organic matter produced by phytoplankton, subsequently affecting bacterial degradation, zooplankton reproduction and the biomass export to the deep ocean. Therefore, changes in the C:N ratios have further implications for marine ecosystem dynamics and are critical to the response of the ocean to global change (Riebesell et al. 2007; Finkel et al. 2010). In *T. pseudonana*, NO_3^- and high CO_2 worked interactively to increase the C: N ratio, but as the ocean is expected to have higher CO_2 but less NO_3^- in the future the effects of environmental change on C:N ratio may largely offset in this diatom.

It should be noted, however, that there are certainly species-specific response of energy metabolism and thus cellular biochemical and elemental composition to the changes in environmental factors (e.g., elevated pCO_2, shifting of nitrogen source, and increasing irradiance) (Thompson et al. 1990; Levasseur et al. 1993; Reinfelder 2012; Leu et al. 2013; Trimborn et al. 2013; Wynn-Edwards et al., 2014). The underlying mechanisms of how different phytoplankton species respond and acclimate to the concurrently changing conditions are mostly unclear. Moreover, at community level, the changes of environmental factors are often linked to change in taxonomic composition (Riebiesell et al. 2007; Leu et al. 2013). Therefore, caution should be taken to extrapolate the conclusion obtained at organism levels to community level, and more research on the mechanisms of species-specific response of marine phytoplankton to the changing ocean is certainly in need.

References

Alexandre, A., J. Silva, P. Buapet, M. Bjork, and R. Santos. 2012. Effects of CO_2 enrichment on photosynthesis, growth, and nitrogen metabolism of the seagrass *Zostera noltii*. Ecol. Evol. **2**: 2620–2630. doi:10.1002/ece3.333

Allen, A. P., J. F. Gilooly, and J. H. Brown. 2005. Linking the global carbon cycle to individual metabolism. Funct. Ecol. **19**: 202–213. doi:10.1111/j.1365-2435.2005.00952.x

Badger, M. R., T. J. Andrews, S. M. Whitney, M. Ludwig, D. C. Yellowlees, W. Leggat, and G. D. Price. 1998. The diversity and coevolution of Rubisco, plastids, pyrenoids, and chloroplast-based CO_2-concentrating mechanisms in algae. Can. J. Bot. **76**: 1052–1071. doi:10.1139/b98-074

Beardall, J. 1989. Photosynthesis and photorespiration in marine phytoplankton. Aquat. Bot. **34**: 105–130. doi: 10.1016/0304-3770(89)90052-1

Behrenfeld, M. J., and others. 2006. Climate-driven trends in contemporary ocean productivity. Nature **444**: 752–755. doi:10.1038/nature05317

Beman, J. M., and others. 2011. Global declines in oceanic nitrification rates as a consequence of ocean acidification. Proc. Natl. Acad. Sci. USA **108**: 208–213. doi:10.1073/pnas.1011053108

Bender, S. J., M. S. Parker, and E. V. Armbrust. 2012. Coupled effects of light and nitrogen source on the urea cycle and nitrogen metabolism over a diel cycle in the marine diatom *Thalassiosira pseudonana*. Protist **163**: 232–251. doi:10.1016/j.protis.2011.07.008

Berges, J. A., and P. J. Harrison. 1995a. Nitrate reductase activity quantitatively predicts the rate of nitrate incorporation under steady-state light limitation—a revised assay and characterization of the enzyme in 3 species of marine phytoplankton. Limnol. Oceanogr. **40**: 82–93. doi:10.4319/lo.1995.40.1.0082

Berges, J. A., and P. J. Harrison. 1995b. Relationships between nitrate reductase activity and rates of growth and nitrate incorporation under steady-state light or nitrate limitation in the marine diatom *Thalassiosira pseudonana* (Bacillariophyceae). J. Phycol. **31**: 85–95. doi:10.1111/j.0022-3646.1995.00085.x

Bloom, A. J. 2015. Photorespiration and nitrate assimilation: A major intersection between plant carbon and nitrogen. Photosynth. Res. **123**: 117–128. doi:10.1007/s11120-014-0056-y

Boyd, P. W., and D. A. Hutchins. 2012. Understanding the responses of ocean biota to a complex matrix of cumulative anthropogenic change. Mar. Ecol. Prog. Ser. **470**: 125–135. doi:10.3354/meps10121

Boyd, P. W., R. Strzepek, F. Fu, and D. A. Hutchins. 2010. Environmental control on open-ocean phytoplankton groups: Now and in the future. Limnol. Oceanogr. **53**: 1353–1376. doi:10.4319/lo.2010.55.3.1353

Breitbarth, E., and others. 2010. Ocean acidification affects iron speciation during a coastal seawater mesocosm experiment. Biogeosciences **7**: 1065–1073. doi:10.5194/bg-7-1065-2010

Broecker, W. S. 1982. Ocean geochemistry during glacial time. Geochim. Cosmochim. Acta. **46**: 1689–1705. doi:10.1016/0016-7037(82)90110-7

Caldeira, K., and M. Wickett. 2003. Anthropogenic carbon and ocean pH. Nature **425**: 365. doi:10.1038/425365a

Campbell, D. A., Z. Hossain, A. M. Cockshutt, O. Zhaxybayeva, H. Wu, and G. Li. 2013. Photosystem II protein clearance and FstH function in the diatom *Thalassiosira pseudonana*. Photosynth. Res. **115**: 43–54. doi:10.1007/s11120-013-9809-2

Collins, S., B. Rost, and T. A. Rynearson. 2014. Evolutionary potential of marine phytoplankton under ocean acidification. Evol. Appl.**7**: 140–155. doi:10.1111/eva.12120

Dickson, A. G., and F. J. Millero. 1987. A Comparison of the equilibrium constants for the dissociation of carbonic acid in seawater media. Deep-Sea Res. **34**: 1733–1743. doi:10.1016/0198-0149(87)90021-5

Doney, S. C. 2006. Plankton in a warmer world. Nature **444**: 695–696. doi:10.1038/444695a

Doney, S. C., V. J. Fabry, R. A. Feely, and J. A. Kleypas. 2009. Ocean acidification: The other CO_2 problem. Annu. Rev. Mar. Sci. **1**: 169–192. doi:10.1146/annurev.marine.010908.163834

Duce, R. A., and others. 2008. Impacts of atmospheric anthropogenic nitrogen on the open ocean. Science **320**: 893–897. doi:10.1126/science.1150369

Dutkiewicz, S., J. R. Scott, and M. J. Follows. 2013. Winners and losers: Ecological and biogeochemical changes in a warming ocean. Glob. Biogeochem. Cycle **27**: 463–477. doi:10.1002/gbc.20042

Eichner, M., A. K. Kranz, and B. Rost. 2014. Combined effects of different CO_2 levels and N sources on the diazotrophic cyanobacterium *Trichodesmium*. Physiol. Plantarum **152**: 316–330. doi:10.1111/ppl.12172

Falkowski, P. G., and A. R. Raven. 2007. Aquatic Photosynthesis, 2nd ed. Princeton Univ. Press.

Finkel, Z. V., J. Beardall, K. J. Flynn, A. Quigg, T. A. V. Rees, and J. A. Raven. 2010. Phytoplankton in a changing world: Cell size and elemental stoichiometry. J. Plankton Res. **32**: 119–137. doi:10.1093/plankt/fbp098

Fogg, G. 1983. The ecological significance of extracellular products of phytoplankton photosynthesis. Bot. Mar. **26**: 3–14. doi:10.1515/botm.1983.26.1.3

Frada, M. J., E. H. Burrows, K. D. Wyman, and P. G. Falkowski. 2013. Quantum requirements for growth and fatty acid biosynthesis in the marine diatom *Phaeodactylum tricornutum* (Bacillariophyceae) in nitrogen replete and limited conditions. J. Phycol. **49**: 381–388. doi:10.1111/jpy.12046

Gao, K., and D. A. Campbell. 2014. Photophysiological responses of marine diatoms to elevated CO_2 and decreased pH: A review. Funct. Plant Biol. **41**: 449–459. doi:10.1071/FP13247

Gao, K. S., and others. 2012. Rising CO_2 and increased light exposure synergistically reduce marine primary productivity. Nat. Clim. Change **2**: 519–523. doi:10.1038/nclimate1507

Garcia, H. E., and L. I. Gordon. 1992. Oxygen solubility in seawater: Better fitting equations. Limnol. Oceanogr. **37**: 1307–1312. doi:10.4319/lo.1992.37.6.1307

Granum, E., and S. M. Myklestad. 2002. A simple combined method for determination of beta-1,3-glucan and cell wall polysaccharides in diatoms. Hydrobiologia **477**: 155–161. doi:10.1023/A:1021077407766

Halsey, K. H., and B. M. Jones. 2015. Phytoplankton stratigies for photosynthetic energy allocation. Annu. Rev. Mar. Sci. **7**: 265–297. doi:10.1146/annurev-marine-010814-015813

Hennon, G. M. M., P. Quay, R. L. Morales, L. M. Swanson, and E. V. Armbrust. 2014. Acclimation conditions modify physiological response of the diatom *Thalassiosira pseudonana* to elevated CO_2 concentrations in a nitrate-limited chemostat. J. Phycol. **50**: 243–253. doi:10.1111/jpy.12156

Hofmann, L. C., S. Straub, and K. Bischof. 2013. Elevated CO_2 levels affect the activity of nitrate reductase and carbonic anhydrase in the calcifying rhodophyte *Corallina officinalis*. J. Exp. Bot. **64**: 899–908. doi:10.1093/jxb/ers369

Hopkinson, B. M., C. L. Dupont, A. E. Allen, and F. M. M. Morel. 2011. Efficiency of the CO_2-concentrating mechanism of diatoms. Proc. Natl. Acad. Sci. USA **108**: 3830–3837. doi:10.1073/pnas.1018062108

Huesemann, M. H., A. D. Skillman, and E. A. Crecelius. 2002. The inhibition of marine nitrification by ocean disposal of carbon dioxide. Mar. Pollut. Bull. **44**: 142–148. doi:10.1016/S0025-326X(01)00194-1

Koch, M., G. Bowes, C. Ross, and X. H. Zhang. 2013. Climate change and ocean acidification effects on seagrasses and marine macroalgae. Glob. Change Biol. **19**: 103–132. doi:10.1111/j.1365-2486.2012.02791.x

Leboulanger, C., L. Oriol, H. Jupin, and C. Descolas-Gros. 1997. Diel variability of glycolate in the eastern tropical Atlantic Ocean. Deep-Sea Res. Part I **44**: 2131–2139. doi:10.1016/S0967-0637(97)00090-3

Leu, E., M. Daase, K. G. Schulz, A. Stuhr, and U. Riebesell. 2013. Effect of ocean acidification on the fatty acid composition of a natural plankton community. Biogeosciences **10**: 1143–1153. doi:10.5194/bg-10-1143-2013

Levasseur, M., P. A. Thompson, and P. J. Harrison. 1993. Physiological acclimation of marine phytoplankton to different nitrogen sources. J. Phycol. **29**: 587–595. doi:10.1111/j.0022-3646.1993.00587.x

Li, G., and D. A. Campbell. 2013. Rising CO_2 interacts with growth light and growth rate to alter photosystem II photoinactivation of the coastal diatom *Thalassiosira pseudonana*. Plos One **8**: e55562. doi:10.1371/journal.pone.0055562

Li, G., C. M. Brown, J. A. Jeans, N. A. Donaher, A. McCarthy, and D. A. Campbell. 2014. The nitrogen costs of photosynthesis in a diatom under current and future pCO_2. New Phytol. **205**: 533–543. doi:10.1111/nph.13037

Litchman, E., K. F. Edwards, C. A. Klausmeier, and M. K. Thomas. 2012. Phytoplankton niches, traits and eco-evolutionary responses to global environmental change. Mar. Ecol. Prog. Ser. **470**: 235–248. doi:10.3354/meps09912

Lomas, M. W. 2004. Nitrate reductase and urease enzyme activity in the marine diatom *Thalassiosira weissflogii* (Bacillariophyceae): Interactions among nitrogen substrates. Mar. Biol. **144**: 37–44. doi:10.1007/s00227-003-1181-x

Lomas, M. W., and P. M. Glibert. 1999. Temperature regulation of nitrate uptake: A novel hypothesis about nitrate uptake and reduction in cool-water diatoms. Limnol. Oceanogr. **44**: 556–572. doi:10.4319/lo.1999.44.3.0556

Lomas, M. W., C. J. Rumbley, and P. M. Glibert. 2000. Ammonium release by nitrogen sufficient diatoms in response to rapid increases in irradiance. J. Plankton Res. **22**: 2351–2366. doi:10.1093/plankt/22.12.2351

Lopez-Urrutia, A., E. San Martin, R. P. Harris, and X. Irigoien. 2006. Scaling the metabolic balance of the oceans. Proc. Natl. Acad. Sci. USA **103**: 8739–8744. doi:10.1073/pnas.0601137103

McGinn, P. J., and F. M. M. Morel. 2008. Expression and regulation of carbonic anhydrases in the marine diatom *Thalassiosira pseudonana* and in natural phytoplankton assemblages from Great Bay, New Jersey. Physiol. Plantarum **133**: 78–91. doi:10.1111/j.1399-3054.2007.01039.x

Mehrbach, C., C. H. Culberso, J. E. Hawley, and R. M. Pytkowic. 1973. Measurement of apparent dissociation constants of carbonic acid in seawater at atmospheric pressure. Limnol. Oceanogr. **18**: 897–907. doi:10.4319/lo.1973.18.6.0897

Muller, E. B., and R. M. Nisbet. 2014. Dynamic energy budget modeling reveals the potential of future growth and calcification for the coccolithophore *Emiliania huxleyi* in an acidified ocean. Glob. Change Biol. **20**: 2031–2038. doi:10.1111/gcb.12547

Mulholland, M. R., and M. W. Lomas. 2008. Nitrogen uptake and assimilation, p. 303–384. *In* D. G. Capone, D. A. Bronk, M. R. Mulholland, and E. J. Carpenter [eds.], Nitrogen in the marine environment. Elsevier Academic Press.

Myers, S. S., and others. 2014. Increasing CO_2 threatens human nutrition. Nature **510**: 139–142. doi:10.1038/nature13179

Nisbet, R. M., M. Jusup, T. Klanjscek, and L. Pecquerie. 2012. Integrating dynamic energy budget (DEB) theory with traditional bioenergetic models. J. Exp. Biol. **215**: 892–902. doi:10.1242/jeb.059675

Norici, A., A. M. Bazzoni, A. Pugnetti, J. A. Raven, and M. Giordano. 2011. Impact of irradiance on the C allocation in the coastal marine diatom *Skeletonema marinoi* Sarno and Zingone. Plant Cell Environ. **34**: 1666–1677. doi:10.1111/j.1365-3040.2011.02362.x

Orr, J., V. Fabry, O. Aumont, L. Bopp, and S. Doney. 2005. Anthropogenic ocean acidification over the twenty-first century and its impact on calcifying organisms. Nature **437**: 681–686. doi:10.1038/nature04095

Parker, M. S., and E. V. Armbrust. 2005. Synergistic effects of light, temperature, and nitrogen source on transcription of genes for carbon and nitrogen metabolism in the centric diatom *Thalassiosira pseudonana* (Bacillariophyceae). J. Phycol. **41**: 1142–1153. doi:10.1111/j.1529-8817.2005.00139.x

Parker, M. S., E. V. Armbrust, J. Piovia-Scott, and R. G. Keil. 2004. Induction of photorespiration by light in the centric diatom *Thalassiosira weissflogii* (Bacillariophyceae): Molecular characterization and physiological consequences. J. Phycol. **40**: 557–567. doi:10.1111/j.1529-8817.2004.03184.x

Pierrot, D., E. Lewis, and D. Wallace. 2006. MS Excel program developed for CO_2 system calculations. Carbon Dioxide Information Analysis Center, Oak Ridge National Laboratory, US Department of Energy.

Raven, J. A., J. E. Kubler, and J. Beardall. 2000. Put out the light, and then put out the light. J. Mar. Biol. Ass. U.K. **80**: 1–25. doi:10.1017/S0025315499001526

Reinfelder, J. R. 2012. Carbon dioxide regulation of nitrogen and phosphorus in four species of marine phytoplankton. Mar. Ecol. Prog. Ser. **466**: 57–67. doi:10.3354/meps09905

Riebesell, U., and others. 2007. Enhanced biological carbon consumption in a high CO_2 ocean. Nature **450**: 545–548. doi:10.1038/nature06267

Roberts, K., E. Granum, R. C. Leegood, and J. A. Raven. 2007. C3 and C4 pathways of photosynthetic carbon assimilation in marine diatoms are under genetic, not environmental control. Plant Physiol. **145**: 230–235. doi:10.1104/pp.107.102616

Rodriguez-Ruiz, J., E. H. Belarbi, J. L. G. Sanchez, and D. L. Alonso. 1998. Rapid simultaneous lipid extraction and transesterification for fatty acid analyses. Biotechnol. Tech. **12**: 689–691. doi:10.1023/A:1008812904017

Rouco, M., O. Branson, M. Lebrato, and M. D. Iglesias-Rodriguez. 2013. The effect of nitrate and phosphate availability on *Emiliania huxleyi* (NZEH) physiology under different CO_2 scenarios. Front. Microbiol. **4**: 155. doi:10.3389/fmicb.2013.00155

Samukawa, M., C. Shen, B. M. Hopkinson, and Y. Matsuda. 2014. Localization of putative carbonic anhydrases in the marine diatom, *Thalassiosira pseudonana*. Photosyn. Res. **121**: 235–249. doi:10.1007/s11120-014-9967-x

Schaum, E., B. Rost, A. J. Millar, and S. Collins. 2013. Variation in plastic responses of a globally distributed picoplankton species to ocean acidification. Nat. Clim. Change **3**: 298–302. doi:10.1098/rspb.2014.1486

Shi, D., Y. Xu, B. M. Hopkinson, and F. M. M. Morel. 2010. Effect of ocean acidification on iron availability to marine phytoplankton. Science **327**: 676–679. doi:10.1126/science.1183517

Sousa, R., T. Domingos, and S.A.L.M. Kooijman. 2008. From emperical patterns to theory: A formal metabolic theory of life. Phil. Trans. R. Soc. B. **363**: 2453–2464. doi:10.1098/rstb.2007.2230

Subramanian, S., A. N. Barry, S. Pieris, and R. T. Sayre. 2013. Comparative energetics and kinetics of autotrophic lipid and starch metabolism in chlorophytic microalgae: Implications for biomass and biofuel production. Biotechnol. Biofuels **6**: 150. doi:10.1186/1754-6834-6-150

Sukenik, A., J. Bennett, and P. Falkowski. 1987. Light-saturated photosysnthesis—limitation by electron transport of carbon fixation? Biochim. Biophys. Acta **891**: 205–215. doi:10.1016/0005-2728(87)90216-7

Sunda, W. G., and D. R. Hardison. 2007. Ammonium uptake and growth limitation in marine phytoplankton. Limnol. Oceanogr. **52**: 2496–2506. doi:10.4319/lo.2007.52.6.2496

Sunda, W. G., N. M. Price, and F. M. M. Morel. 2005. Trace metal ion buffers and their use in culture studies, p. 35–63. *In* R. A. Andersen [ed.], Algal culturing techniques. Elsevier Academic Press.

Thompson, P. A., P. J. Harrison, and J. N. C. Whyte. 1990. Influence of irradiance on the fatty acid composition of phytoplankton. J. Phycol. **26**: 278–288. doi:10.1111/j.0022-3646.1990.00278.x

Tortell, P. D., and others. 2008. CO_2 sensitivity of Southern Ocean phytoplankton. Geophys. Res. Lett. **35**: L04605. doi:10.1029/2007gl032583

Trimborn, S., T. Brenneis, E. Sweet, and B. Rost. 2013. Sensitivity of Antarctic phytoplankton species to ocean acidification: Growth, carbon acquisition, and species interaction. Limnol. Oceanogr. **58**: 997–1007. doi:10.4319/lo.2013.58.3.0997

Wingler, A., P. J. Lea, W. P. Quick, and R. C. Leegood. 2000. Photorespiration: Metabolic pathways and their role in stress protection. Phil. Trans. R. Soc. B. **355**: 1517–1529. doi:10.1098/rstb.2000.0712

Wu, H., A. M. Cockshutt, A. McCarthy, and D. A. Campbell. 2011. Distinctive photosystem II photoinactivation and protein dynamics in marine diatoms. Plant Physiol. **156**: 2184–2195. doi:10.1104/pp.111.178772

Wynn-Edwards, and others. 2014. Species-specific variations in the nutritional quality of Southern Ocean phytoplankton in response to elevated pCO_2. Water **6**: 1840–1859. doi:10.3390/w6061840

Xia, J. R., and K. S. Gao. 2005. Impacts of elevated CO_2 concentration on biochemical composition, carbonic anhydrase, and nitrate reductase activity of freshwater green algae. J. Integr. Plant Biol. **47**: 668–675. doi:10.1111/j.1744-7909.2005.00114.x

Xu, Y., D. Shi, L. Aristilde, and F. Morel. 2012. The effect of pH on the uptake of zinc and cadmium in marine phytoplankton: Possible role of weak complexes. Limnol. Oceanogr. **57**: 293–304. doi:10.1021/es300335u

Zhang, H., and R. H. Byrne. 1996. Spectrophotometric pH measurements of surface seawater at in-situ conditions: Absorbance and protonation behavior of thymol blue. Mar. Chem. **52**: 17–25. doi:10.1016/0304-4203(95)00076-3

Acknowledgments

We thank Meng Chen for technical assistance with fatty acid measurements and Baiyun Wang for assistance with ^{15}N analysis. We would also like to thank Douglas Campbell and another three anonymous reviewers for helpful and constructive comments on the manuscript. This work was supported by the National Science Foundation of China (No. 41222040), the Fundamental Research Funds for the Central Universities (No. 20720140504), the Recruitment Program of Global Youth Experts of China, and the U.S. National Science Foundation (EF-1041034).

Submitted 20 March 2015
Revised 8 May 2015; 17 June 2015
Accepted 20 June 2015

Associate editor: Susanne Menden-Deuer